HHS Public Access

Author manuscript

*Placenta*. Author manuscript; available in PMC 2017 February 01.

Published in final edited form as:

*Placenta*. 2016 February ; 38: 57–66. doi:10.1016/j.placenta.2015.12.011.

# In-vivo Stretch of Term Human Fetal Membranes

**EM Joyce**[1], **P Diaz**[2,3], **S Tamarkin**[2], **R Moore**[4], **A Strohl**[4], **B Stetzer**[5], **D Kumar**[4], **MS Sacks**[6], and **JJ Moore**[4,5]

[1]Department of Bioengineering, Swanson School of Engineering, School of Medicine, University of Pittsburgh, Pittsburgh PA, USA

[2]Department of Radiology, MetroHealth Medical Center and Case Western Reserve University, USA

[3]Department of Biomedical Engineering, Case Western Reserve University, USA

[4]Department of Pediatrics, MetroHealth Medical Center and Case Western Reserve University, USA

[5]Department of Reproductive Biology, MetroHealth Medical Center and Case Western Reserve University, Cleveland, OH, USA

[6]Department of Biomedical Engineering and the Institute for Computational Engineering and Sciences, The University of Texas at Austin, Austin, TX 78712-0027, USA

## Abstract

**Introduction—**Fetal membranes (FM) usually fail prior to delivery during term labor, but occasionally fail at preterm gestation, precipitating preterm birth. To understand the FM biomechanical properties underlying these events, study of the baseline *in-vivo* stretch experienced by the FM is required. This study's objective was to utilize high resolution MRI imaging to determine *in-vivo* FM stretch.

**Methods—**Eight pregnant women (38.4±0.4wks) underwent abdominal-pelvic MRI prior to (2.88±0.83d) caesarean delivery. Software was utilized to determine the total FM *in-vivo* surface area (SA) and that of its components: placental disc and reflected FM. At delivery, the SA of the disc and FM in the relaxed state were measured. *In-vivo* (stretched) to delivered SA ratios were calculated. FM fragments were then biaxially stretched to determine the force required to re-stretch the FM back to *in-vivo* SA.

**Results—**Total FM SA, *in-vivo* vs delivered, was 2135.51±108.47 $cm^2$ vs 842.59±35.86 $cm^2$; reflected FM was 1778.42±107.39 $cm^2$ vs 545.41±22.90 $cm^2$, and disc was 357.10±28.08 $cm^2$ vs 297.18±22.14 $cm^2$. The ratio (*in-vivo* to *in-vitro* SA) of reflected FM was 3.26±0.11 and disc was 1.22±0.10. Reflected FM re-stretched to *in-vivo* SA generated a tension of 72.26N/m,

Corresponding Author and Reprint Requests: John J. Moore MD, Professor of Pediatrics and Reproductive Biology, Case Western Reserve School of Medicine, MetroHealth Campus, 2500 MetroHealth Drive, Cleveland OH 44109, Phone 216-778-5946; jmoore@metrohealth.org; jjm6@case.edu.

Location where study was performed: MetroHealth Medical Center, Cleveland, Ohio and Department of Biomedical Engineering, Pittsburgh, PA

Conflict of Interest: Authors have no conflict of interest to declare.

corresponding to approximate pressure of 15.4mmHg. FM rupture occurred at 295.08 ± 31.73N/m corresponding to approximate pressure of 34mmHg. Physiological SA was 70% of that at rupture.

**Discussion—**FM are significantly distended *in-vivo*. FM collagen fibers were rapidly recruited once loaded and functioned near the failure state during *in-vitro* testing, suggesting that, *in-vivo*, minimal additional (beyond physiological) stretch may facilitate rapid, catastrophic failure.

### Keywords

fetal membranes; surface area; MRI; deformation; intrauterine stretch; biomechanics

## Introduction

Normal pregnancy requires that the physical integrity of the fetal membranes (FM) be maintained until term delivery. However, premature failure of the FM-aka preterm premature of fetal membranes is responsible for nearly 40% of all preterm births. Preterm birth is a major global public health problem with an estimated 14.9 million babies being born premature in 2010 worldwide[1]. Prematurity is responsible for 35% of the world's 3.1 million annual neonatal deaths and is the second largest direct cause of deaths in children less than 5 years.[2] Preterm birth rate in the US is high at 11.39 % resulting in US being one of the ten countries globally with highest number of preterm births.[1,3]

The physiological mechanisms which cause membranes to fail, term or preterm, are not completely understood. In the past, weakening and rupture of the FM were attributed to the mechanical stresses of labor contractions. This is clearly inconsistent with the 10% of term and 40% of preterm births in which FM rupture precedes contractions. It is now established that FM weaken in late gestation as a result of biochemical changes: extracellular matrix remodeling and apoptosis in late gestation.[4] Many groups have confirmed that these biochemical changes are focused at the para-cervical zone of FM overlying the cervix.[4,5-18] We have further demonstrated that this biochemically remodeled, para-cervical FM region is physically weaker than other FM regions and have termed it “physiological weak zone”.[4,12,13] The spontaneous rupture of FM initiates in this physiological weak zone but it is not clear how this occurs.

The FM is a collagenous soft tissue that surrounds the fetus with a major role in supporting the fetus and amniotic fluid, and in tolerating local deformation associated with fetal movements during gestation.[19,20] The FM is a complex structure with two components; the choriodecidua which is relatively thick and cellular, and the amnion which is thinner and stronger. The amnion accounts for approximately 20% of the FM thickness but dominates the mechanical response of the FM.[21,22] In-*vitro*, the amnion undergoes a decrease in thickness with substantial collagen fiber alignment in response to minimal loads.[23] Type I collagen in the compact sublayer of the amnion is responsible for much of the mechanical strength of the FM.

Individual collagen fibers are initially undulated (crimped) in a stress-free state.[24] Undulated collagen fibers do not carry load, but once a fiber has been stretched to a “straightened” state, the fiber will transmit load in a linearly elastic manner (Figure 1). Stretch can be

defined as: $\lambda=L/L_o$, where L is the current (stretched) length of the collagen fiber and $L_o$ is the original length of the collagen fiber before being stretched (Figure 1). FM collagen fibers are recruited at different stretch levels due to various degrees of initial collagen crimping (Figure 1). While one fiber may be fully stretched, another may still be crimped, resulting in a non-linear tension-stretch curve (Figure 1). Once all collagen fibers are straightened, the tension-stretch curve becomes linear. In this region, membrane tension can be defined as force/unit length (Figure 1). When a small number of fibers are present, the various regions of the tension-stretch curve (i.e. "toe" region, transition regions between the "toe" and linear regions, highly linear region) are discrete (Figure 1; solid line). However, when a large population of fibers is present, the tension-stretch curve is continuous, as demonstrated previously by Oyen *et al*. (Figure 1; dashed line).[19-21]

Tissue failure (rupture), which occurs when the FM can stretch no further, is a unique event in normal human physiology. Other tissue failures (e.g. bone fracture, skin tears, vascular aneurysms) are all pathological processes. Because tissue failure typically occurs as a result of a pathological process and not normal function, the biomechanics of soft tissue failure is generally poorly understood. The importance of biomechanics in FM failure is reflected in the relation between biomechanical and biochemical processes. Millar *et al*. have suggested that distention of the FM extracellular matrix (ECM) normally stimulates remodeling of the ECM, resulting in an increase in membrane surface although there is minimal growth of the FM during the final weeks of pregnancy as demonstrated by decreased mitosis[25]. Excessive distension or inadequate remodeling, could result in preterm premature rupture of the FM and preterm birth.[26] We have demonstrated in both clinical human FM specimens, and from our *in-vitro* human FM weakening model, that FM remodeling associated with collagen degradation and cellular apoptosis plays an important role in FM weakening.[4,12,13,27-33] Biochemically pre-weakened FM more readily fail as a result of the mechanical forces of uterine contractions at the onset of labor. This is supported by the known interplay between mechanical deformation and collagen degradation in other collagenous soft tissues both of which perhaps works synergistically to induce tissue failure.[34-37] Ellsmere *et al*. demonstrated that tensile loading accelerates the proteolysis of bovine pericardium subjected to collagenase, while another study demonstrated that the degradation rate of collagen increased with stretch.[34,36]

In order to develop a rational basis for treatment and prevention of premature FM failure, a better understanding of FM structural and mechanical behavior at near/full term under both sub-failure and failure conditions is necessary. In order to quantify the intact FM (FM with amnion adherent to the choriodecidua) mechanical behavior under sub-failure and failure conditions from full term tissues, it is necessary to perform this ordered sequence: (1) Accurately measure baseline FM stress *in-vivo* in order to determine its effects on growth and failure of the FM; (2) Quantify the FM mechanical properties under biaxial stretch; (3) Use the biaxial stretch data to develop a structural (mathematical) model to derive intrinsic fiber properties; and (4) Use the model to gain insight into the micromechanical mechanisms of failure. To initiate this, intrauterine physiological tension of the FM was determined utilizing a two-step procedure. First, the areal stretch, the ratio of the surface area of the FM *in-vivo* (at term just prior to delivery) vs *in-vitro* surface area (immediately after delivery)

was determined. Second, fragments of FM were biaxially stretched with a novel membrane inflation device to provide tension-areal stretch data from sub-failure to failure. The surface area ratio obtained in the first step was used to interpolate the intrauterine stress from this tension-areal stretch data.

## Methods

### Tissue procurement

The protocols for this study were approved by the Institutional Review Board at MetroHealth Medical Center/Case Western Reserve University. Informed consent was obtained from all participants. FMs were obtained from term pregnant (mean gestational age of 38.41±0.36 weeks) women delivering in the MetroHealth Medical Center by repeat Cesarean Section. The patients had no pregnancy complications and underwent Cesarean deliveries only because of a previous Cesarean delivery. Patients were scheduled for MRI within several days (0-7) of the scheduled delivery (average number of days between MRI and delivery = 2.88±0.83). The MRI data from these patients were used to determine the *in-vivo* surface area measurements. *In-vitro* FM surface area measurements were performed immediately following delivery

### In-vivo surface area measurement

T2-weighted fast breath hold sequences were utilized to generate isotropic MRI images throughout the placenta and FM. The MRI images (Figure 2a) were then segmented (Figure 2b) using free software, Medical Image Processing, Analysis, and Visualization (MIPAV), from the NIH website (http://mipav.cit.nih.gov/). Each MRI image was segmented and stacked (Fig. 2c). The resulting segmented images (Figure 2c) were then imported into Geomagic/Studio (Research Triangle Park, NC), a commercial software package, in order to produce a three-dimensional cloud of points, commonly referred to as a point cloud (Figure 2d). The point cloud data derived from segmentation served as a link between MRI and a three-dimensional geometric model. Next, a surface wrap was performed to produce a stereolithography (STL) formatted surface (Figure 2e). A STL surface is a simple surface definition made by triangulating the point cloud data, which produces a set of triangular elements that only contains information of connectivity and surface normals (Figure 2f). The STL surface was then conservatively smoothed because raw data can lead to imperfections in the geometric quality. Next, four sided patches were defined which capture significant topological and curvature surface characteristics. A Non Uniform Rational B-spline (NURBs) based model was then constructed from the patch definition by establishing a grid of control points within the field of patches (Figure 2g). The NURBs format is compatible with CAD modeling tools such as SolidWorks (Dassault Systemes SolidWorks Corp. Concord, MA). After the NURBs-based geometry was constructed, SolidWorks was used to calculate the *in-vivo* FM surface area. In addition to the total gestational sack surface area, the surface area of the placental amnion (covering the disc) was separately determined. The reflected FM SA was then the total minus the disc area.

### In-vitro surface area measurements

Upon receipt of the placenta and FM, the membranes were carefully dissected from the placental disc as close to the placental rim as possible. The reflected FM was washed in room temperature phosphate buffered saline (PBS) and carefully cut into three or four fragments. Note, the number of fragments used was sufficient to flatten the membranes with no apparent residual curvature or wrinkling. The fragments were maintained in room temperature PBS for 10-15 minutes while the disc was traced. Tracing involved placing the placental disc in a dish fetal side up. The pan was covered with a plexiglass plate (plate does not touch the disc) and a marker was used to carefully trace the placental (amnion covered) disc area onto the plexiglass. This tracing was then transferred to tracing paper. Each of the FM fragments was then gently placed on a shallow flat tray which was filled with room temperature PBS to a depth of approximately 0.5 cm. Once filled, the FM fragments were suspended in the PBS in slight contact with the bottom of the tray. The FM fragments (if contorted) were carefully unfolded into single layers, amnion side facing down (toward the bottom of the tray). The tray was gently agitated for 30-40 seconds resulting in spreading and suspension of the FM fragments. The PBS was removed from the tray by vacuum aspiration leaving the wet FM fragment lying on the bottom of the tray in the same conformation as when suspended. The plexiglass sheet was then placed over the tray without touching the FM and the area of each fragment was traced onto the plexiglass, then transferred to tracing paper as outlined above for the disc.

To calculate the post-delivery surface area from the tracings, four 10 cm × 10 cm pieces of tracing paper were carefully measured and cut out. The four fragments of tracing paper were weighed, and the average weight for a 100 $cm^2$ area was determined. Then, the placental disc tracing and the FM fragment tracings were cut out. The tracings were then weighed, and the surface areas of each tracing were determined by comparing their weights against the "standard" calculated above. Note that for these studies, only the amnion surface of the placental disc was included in the surface area measurements. The disc was traced because the surface area of the placental amnion over the disc needed to be measured, and separating this tissue from the placenta would have severely stretched the amnion.

### Physiological membrane deformation analysis

In order to estimate the *in-vivo* stretch of the FM, the surface area determined from the *in-vivo* measurements was divided by the *in-vitro* surface area measurements:

$$\text{Areal Stretch} = \frac{in-vivo\ \text{surface area}}{in-vivo\ \text{surface area}} \quad (1)$$

### Membrane inflation study

Membrane inflation studies were performed on post-delivered intact FM in order to produce a FM tension-areal stretch curve, allowing direct correlation between *in-vivo* areal stretch, which was determined from the MRI, and the corresponding membrane tension. They were also performed on the amnion layer to gain insight into the FM failure process.

A novel membrane inflation device was developed in order to perform membrane failure tests on the FM by means of equi-biaxial stretch loading while simultaneously quantifying collagen fiber architecture of the amnion layer during loading. The device consisted of a pressure chamber with imaging windows and specimen holder. PBS was utilized to apply sufficient pressure to induce failure (Figure 3A, B, and C). Pressure is applied with a syringe pump and was monitored with a pressure transducer, and small angle light scattering (SALS) was used to nondestructively quantify the collagen fiber architecture as pressure was incrementally applied. A detailed description of the SALS technique has been previously reported.[38,39] Briefly, a 4 mW HeNe continuous unpolarized laser ($\lambda$ = 632.8 nm) was passed through the tissue specimen. The spatial intensity distribution of the resulting scattered light represented the sum of all structural information within the light beam envelope. The angular distribution of scattered light pattern, I($\Phi$), which represented distribution of fiber angles within light beam envelope, was obtained. Quantifiable information based on I($\Phi$) included orientation index (OI), which is defined as the angle that contains one half of the total area under the I($\Phi$) distribution. Normalized orientation index (NOI) was calculated using:

$$\mathrm{NOI}=\frac{90^{\circ}-\mathrm{OI}}{90^{\circ}}\times 100 \quad (2)$$

where NOI ranged from 0% for a complete random network to 100% for a perfectly aligned network.[38] Pressure and axial displacement were measured and recorded.

Full thickness FM tissue fragments selected to be away from the paracervical weak zone FM (n = 4, each fragment from a different FM) were utilized for these experiments.[4,12,13] The FM was first cut into a circular shape approximately 10-13 cm in diameter. This ensured that the sample was large enough to be securely fastened between the clamping plates of the membrane inflation device (Figure 3A, 3B, and 3C). Hollow cylinder 1 was filled with PBS (pH 7.4) at room temperature, and the circular FM section was then placed on top of the clamping plate 1 connected to cylinder 1. Next, hollow cylinder 2 attached to clamping plate 2 was filled with PBS and hollow cylinder 1 attached to clamping plate 1 was then fastened to clamping plate 2, securing the FM between both clamping plates. Note, both clamping plates contained a series of interlocking grooves, which served to align the clamping plates as well as hold the FM in place. In to the interlocking grooves, each clamping plate contained two o-ring grooves, where o-rings were placed in each groove in order to grip the membrane and prevent slippage as well as to serve as a seal to the atmosphere. Finally, the device was placed in its cradle. A three-way stop cock was connected to the side of cylinder 2, and a syringe pump and pressure transducer were connected to ports of the stop cock. PBS was chosen as the means to apply pressure on the FM, and a blood pressure transducer (BLPR2) with an operating range between -50 to +300 mmHg (Sarasota, FL) monitored the pressure level up to failure. Pressure was applied continuously using a syringe pump (Harvard Apparatus PHD 2000 Syringe Pump) until membrane rupture. Pressure was recorded and axial images were taken of the FM during inflation in order to determine the displacement of the center of the inflated membrane. This is a necessary requirement for the determination of the membrane tension and the areal stretch as discussed below.

Because the amnion layer of the FM is largely composed of collagen and because it is the major strength bearing component of the FM[21,22], collagen fiber architecture measurements were performed on the amnion layer. Samples (n = 6, each from a different FM) were prepared by separating the amnion layer from the intact FM, and then tested with the membrane inflation device, as described above. Specifically, collagen fiber architecture was measured at 0 mmHg, 5 mmHg, 20 mmHg, 50 mmHg, 100 mmHg, after which it was measured in 10mmHg pressure increments until membrane rupture.

### Stress-Stretch analysis of membrane

A hollow cylinder within hollow cylinder 2 exists in order to deform the FM into a known geometry, allowing one to easily compute the membrane stresses within the FM (Figure 4A). In order to ensure that the FM was deforming uniformly, validation studies were first performed on latex, an assumed isotropic material, and then on the intact FM. For the validation study, images were taken of the profiles of inflated latex from the top view and side view of the burst device, which were then segmented with free software, Medical Image Processing, Analysis, and Visualization (MIPAV), from the NIH website (http://mipav.cit.nih.gov/). Next, the pixel coordinates from the surface of the segmented images were extracted and plotted for comparison. The $R^2$ value between the two profile curves was 0.9105, where any difference in the plotted curves can be contributed to experimental error associated with manual segmentation of the profile images and image quality. Next, the amnion was inflated until the total displacement was of the amnion was ∼15mm, since pilot study revealed that the amnion ruptured at a displacement of ∼18-20 mm. Through the same analysis, the $R^2$ value between the two profile curves was 0.9398, where any difference in the plotted curves can be contributed to experimental error associated with manual segmentation of the profile images and image quality. Thus, it was concluded from the validation studies that both the latex material and the FM deformed similarly and uniformly.

Due to the constrained geometry of the deformed FM and the deformed state of the FM, assumptions about the deformation of the FM during burst testing can be made. The deformation assumption utilized in the analysis of cells during micropipette aspiration was thus exploited[40]. In micropipette analysis, it is assumed that the equilibrium shapes of an aspirated cell or, in this case, the FM, are composed of spherical and cylindrical parts. In the case of a cell, as aspiration proceeds, the cell projection into the pipette grows, where the radius of the pipette is $R_1$, the radius of the spherical part of the cell in the pipette is $R_2$, and the projection length of the cell is L. This same approach was applied to the FM during the membrane inflation studies, where $R_1$ is the diameter of the inner wall of the membrane inflation device (1.5 cm, Figure 3C), $R_2$ is the radius of the FM, and L is the measured displacement of the center the inflated FM. Displacement of the center of the inflated FM was determined from the sequential axial images taken at each pressure value during inflation. In the case when $L<R_1$, the geometry of the intact FM was treated as an oblate spheroid, or an elliptical membrane. However, when the $L \geq R_1$, the projection length continues to increase as a cylinder with a hemispherical cap with the same radius as the pipette, $R_1$, and $R_1 = R_2$. The principal stress resultants for an inflated elliptical membrane can be defined as: $T_1 = \frac{Pa^2}{2(a^2\sin^2\phi + b^2\cos^2\phi)^{\frac{1}{2}}}$ and

$$T_2 = \frac{Pa^2}{(a^2\sin^2\phi + b^2\cos^2\phi)^{\frac{1}{2}}}\left(1 - \frac{a^2\sin^2\phi + b^2\cos^2\phi}{2b^2}\right) \quad (3)$$

$T_1$ and $T_2$ are the meridional (Figure 4B) and circumferential (Figure 4B) stress resultants, respectively, *P* is the distension pressure, and *a* and *b* are the deformed principal radii. *a* is the radius of the deformed membrane, which is determined from the displacement of the center of the inflated FM, and *b* is the radius of the membrane inflation device (1.5 cm). $\Phi$ is the angle formed between any point on the inflated membrane and center of the inflated membrane and ranges from 0° to 90°. When *a* = *b*, equation 3 reduces to the results for an inflated spherical membrane:

$$T_1 = T_2 = \frac{Pa}{2} \quad (4)$$

as in the case of micropipette aspiration. Thus, when the projection length L was less than 1.5 cm, equation 3 will be employed, and when L is greater or equal to 1.5 cm, equation 4 was employed. Note that when the projection length, L, of the FM is less than $R_1$ and the meridional membrane tension and the circumferential membrane tension ($T_1$ and $T_2$, respectively) vary over the surface of the membrane, with the greatest tension at the top of the membrane. In this case, the reported membrane tension is the average of the meridional and the circumferential membrane tension, where:

$$T = \frac{T_{1,average} + T_{2,average}}{2} \quad (5)$$

The areal stretch of the deformed FM can be defined by the deformed FM surface area divided by the undeformed area. Note that due to equi-biaxial stretch conditions, shear stretches are zero and principle stretches are equal. When $L<R_1$, the geometry of the intact FM was treated as an oblate spheroid, or an elliptical membrane, the deformed surface area of the membrane can be defined as:

$$Surface\ Area = 2\pi b^2 + \pi\frac{a^2}{e}\ln\left(\frac{1+e}{1-e}\right), where\ e \equiv \sqrt{1 - \frac{a^2}{b^2}} \quad (6)$$

When the $L \geq R_1$, the surface area of the deformed membrane can be described by the surface area of a hollow cylinder and hemispherical cap:

$$Surface\ Area = 2\pi bh + 2\pi b^2 \quad (7)$$

Thus, the areal stretch can be determined by dividing the deformed surface area of the FM determined from equations (6) or (7) by the undeformed area of the FM, which is defined as a circle:

$$Areal\ Stretch = \begin{cases} \frac{2\pi b^2 + \pi \frac{a^2}{e} \ln\left(\frac{1+e}{1-e}\right)}{\pi b^2} when\ L < R_1 \\ \frac{2\pi r h + 2\pi r^2}{\pi b^2} when\ L \geq R_1 \end{cases} \quad (8)$$

## Results

### Determination of areal stretch

Areal stretch of the FM, the ratio of the surface area of the FM *in-vivo* (at term just prior to delivery) to the *in-vitro* FM surface area (measured immediately after delivery) was initially determined. Eight patients underwent MRI before delivery (range 0-7; mean 2.9 days) by Cesarean Section at term (mean 38.41±0.36; range 36.57-39.85 weeks). The *in-vivo* surface areas of the FM were determined from the MRIs using the process described in Methods and Figure 2. Figure 5 depicts the three dimensional reconstruction of the FM from MRI, which was utilized to determine the *in-vivo* surface areas. The surface area of the delivered gestational sac (i.e. *in-vitro* surface area), which included both the reflected FM and the placental amnion (on the disc surface) was measured as described in Methods. The details for each FM are listed in Table 1.

The *in-vivo* surface area of the placental amnion (disc) was 357.09 ± 28.08 $cm^2$ and that of the reflected FM was 1778.42 ± 107.39 $cm^2$. The *in-vitro* surface area of the placental amnion (disc) was 297.18 ± 22.14 $cm^2$ and the surface area of the reflected FM was 545.41 ± 22.90 $cm^2$. The ratio of the *in-vivo* surface area to the *in-vitro* surface area of the reflected FM (not including disc stretch), or the fold areal stretch *in-vivo*, was 3.26 ± 0.11. The placental disc did not stretch to the extent of the membranes. The ratio of the *in-vivo* surface area to the *in-vitro* surface area of the placental disc was 1.22 ± 0.10.

### Determination of *in-vitro* FM tension

Fragments of FM were biaxially stretched with the apparatus as described in Methods (Figure 3 & 4) to provide tension-areal stretch data from sub-failure to failure. The areal stretch ratio obtained (above) was then used to interpolate the intrauterine stress from this tension-areal stretch data. The FM tension-areal stretch curve displayed a typical “toe” region at lower values of areal stretch, followed by a transition into highly linear, stiff region (note, only data common to all data sets was averaged and plotted) (Figure 6). Using this curve, an *in-vivo* areal stretch of 3.26 ± 0.11 corresponded to a tension level of 72.26 N/m (Figure 6; solid and dashed lines). Additionally, the average intact FM rupture pressure was determined to be 302.63 ± 29.19 mmHg or 295.08 ± 31.73 N/m (Figure 6; red circle and dashed lines).

It is important to note that these pressure values are dependent on device geometry, while the tension values are not. *In-vivo* pressure values would be much less. For example, if one approximates the *in-vivo* geometry of the FM as a sphere with a radius of 13 cm (based on total *in-vivo* surface area of 2135.51 $cm^2$ given in Table 1), a membrane rupture tension of 295.08 ± 31.73 N/m would yield an estimated *in-vivo* rupture pressure of 34 mmHg, based on the Law of LaPlace (Pressure = 2T/a from equation 4). Note, previously reported FM

rupture pressures range from 40 to 393 mmHg (or estimated rupture tensions of 101.95 to 261.98 N/m)[41].

Although the ratio of tension at rupture to normal physiological tension was 4.08, the physiological areal stretch is ∼70% of the total membrane areal stretch (i.e. stretch at rupture). Thus the collagen fibers are close to maximally stretched and have minimal structural reserve under normal physiological conditions. Note that since each sample did not rupture at the same pressure, the average data represents the average response (n=4) up to the point where data exists for each sample (i.e. an areal stretch value of 3.528). These data were then fit with a polynomial equation, and the data was then extrapolated up the rupture pressure, which corresponds to an areal stretch of 4.681 at rupture.

### Quantitative fiber architecture measurements

Under homogenous loading, the collagen fibers of the amnion were not aligned globally in relation to any anatomic structure in the uterus or placenta. Collagen fibers were recruited (uncrimped) rapidly with loading. NOI values, a measure of collagen alignment, showed an increasing trend with increased pressure, although these changes were not found to be statistically significant. Only minimal further deformation occurred after 50 mmHg of pressure, however, as indicated by the small change in the NOI (Figure 7A and B). Finally, failure at the fiber level in the amnion layer of the FM is a catastrophic event. Furthermore, this strictly catastrophic failure at the fiber level in the amnion was evidenced by a clean, rapid tear. This same behavior was corroborated in the *in-vitro* membrane inflation studies, where collagen fibers were fully recruited and stretched under physiological areal stretch (∼70% of the total membrane stretch), and a minimal increase in areal stretch resulted in membrane failure.

## Discussion

Novel methodologies were developed and utilized to determine normal physiologic intrauterine FM deformation and the corresponding *in-vitro* membrane tension at term. Intrauterine FM tension was obtained by: First, using the ratio of the *in-vivo* FM surface area obtained via MRI close to delivery vs the *in-vitro* surface area measured immediately after delivery to calculate the fold change, or areal stretch of FM *in-vivo*; Second, experimentally determining the relationship between FM areal stretch and FM tension with a specially designed FM inflation device; and Finally, identifying the tension corresponding to the intrauterine fold areal stretch from the experimentally determined Tension-Areal Stretch curve (Figure 6). We were also able to determine the FM structural reserve by comparing normal physiological intrauterine stretch with that which caused rupture in the inflation device.

The few previous measurements of fold areal stretch that exist were based on direct measurement of the maternal abdomen or ultrasonography.[26,42] Parry-Jones and Priya assessed the *in-vivo* surface area in women at preterm and term by placing calipers on the abdomen and measured horizontally between the symphysis pubis and the fundus of the uterus at 5 cm intervals.[42] They determined that the ratio of the *in-vivo* surface area to the *in-vitro* surface area (the degree of distension) was 2.1 in term patients. Millar et al. obtained

serial longitudinal images of the uterus of women at preterm and term by ultrasonography.[26] The ultrasound images were then analyzed with custom software to determine the *in-vivo* surface area. They then measured the area of the expelled membranes after delivery. They determined that the ratio of the *in-vivo* surface area to the *in-vitro* surface area was 1.7 ± 0.3. In both of these studies the assumption was made that the placental amnion (overlying the disc) stretched to the same degree as the reflected FM. Using the same assumption our data show a 2.53 ± .06 fold areal stretch, somewhat higher than the preceding studies. With the more correct assumption that the disc, and its adherent placental amnion, stretch minimally (1.22 ± 0.10), the fold areal stretch of the reflected membranes is even larger (3.26 ± 0.11). It is not surprising that these results are different from those found by Parry-Jones and Priya due to utilization of such simple techniques, which resulted in limited precision in their measurements. Additionally, the results of the current study are likely more accurate than the study performed by Millar et al. due to the use of MRI sections as opposed to ultrasound images.

Through the current study, it can be concluded that the FM is distended during late gestation *in-vivo* with an areal stretch of 3.26 ± 0.11, assuming that the placental amnion (disc) stretches minimally (1.22 ± 0.10). These results corroborate the study performed by Millar *et al*, which demonstrated that the FM grows as well as becomes distended as gestation advances.[26] Although the biochemical processes affecting FM weakening have been somewhat clarified, the concomitant effects of mechanical processes that lead to tissue failure are less clear. The manner in which physical stretch acts upon the biochemically weakened membranes which overlay the cervix is not known (as this region of the FM was not tested), but rupture initiation is postulated to occur in this region.[4,12,13] The relatively, highly loaded state of the FM *in-vivo* may facilitate its susceptibility to enzymatic degradation, which has been shown to be augmented with increased load in other collagenous tissues, as discussed previously.[34-37]

Unlike the FM, other membranous soft tissues, such as the pericardium, heart valves, and unidimensional connective tissues such as ligaments often have a large structural reserve. By this we mean that their internal structures are designed so that they can withstand substantial loading beyond those encountered in normal physiological function. This is evidenced by the observation that their physiological loading ranges are well below their failure strengths.[43-48]

For example, native bovine pericardium has a physiological loading range of 0.6-1 MPa (4,500-7,501 mmHg)[43-45] compared with an ultimate tensile strength of 5 to 26 MPa (37,503 to 195,016 mmHg).[46] Native porcine aortic valve leaflet tissue normally functions at 140 kPa (1,050 mmHg) and has an ultimate tensile strength of 600-1200 kPa (4,500-9,000 mmHg). Ligaments are thought to function in the “toe” region and the early portion of the linear region of the stress-strain curve, approximately 1-6.25 Mpa (7,501- 46,879 mmHg) and have an ultimate tensile strength between 4-45 Mpa (30,002- 337,528 mmHg) depending on the age and type of ligament.[47,48] This structural reserve found in these tissues allows them to withstand loadings beyond their normal physiological demands without incurring damage. In contrast, the FM functions near its failure range (i.e. an estimated physiological tension of 72.26 N/m vs. a burst tension of 295.08 N/m), and well into its

linear region of the Tension-Areal Stretch curve. The FM is thus only capable of withstanding a 4-fold increase in stress above the *in-vitro* stress, and *in-vivo* areal stretch is approximately 70% of the total membrane areal stretch which the FM can withstand. Again the FM tissue in the untested weak zone may tolerate much less stress. Minimal stretch past the determined *in-vivo* stretch results in an exponential increase in tension, which likely facilitates failure of the FM at a prescribed time.

The structural measurements further corroborate the biomechanical findings that the FM functions physiologically in highly loaded state and that the highly loaded state of the FM *in-vivo* may facilitate its susceptibility to enzymatic degradation for programmed, biochemically mediated FM weakening of the para-cervical zone of FM overlying the cervix at term. Under homogenous loading, the collagen fibers of the amnion are not aligned globally in relation to any anatomic structure in the uterus or placenta, and the FM is an effectively isotropic material. Additionally, collagen fibers of the amnion layer were recruited rapidly (i.e. largest change in NOI occurred between 0 and 5 mmHg), and due to the equi-biaxial stretch state and since the change in preferred direction was not significant, the increase in fiber alignment was likely due to the uncrimping of the collagen fibers and not fiber re-orientation. Failure at the fiber level in the amnion layer of the FM is a catastrophic event, evidenced by a clean, rapid tear. If failure was not catastrophic and it manifested due to point defects leading to complete failure, small areas of dark blue (indicative of disruption to the fiber network) would begin to appear prior to failure. However, a large dark blue area in the center of the test specimen, which corresponded to the area of rupture, appeared at rupture. These finding suggests that no fibers are predisposed towards failure, meaning that no fiber is weaker than another fiber prior to biochemical weakening, providing a basis for establishing how the structure-function relationship of the FM is altered in the “weak zone.” It is likely that proteolytic enzymes play a role in the weakening of the FM, and these enzymes perhaps work synergistically with mechanical forces to induce tissue failure. [12,49-51]

The baseline values obtained in these studies define the appropriate ranges for applied stresses in future *in-vitro* biomechanical testing of FM. Biomechanical and structural results demonstrated that FM collagen fibers were rapidly recruited with stretch, followed by a distinct linear region and rapid, catastrophic failure. As a whole, it is apparent that collagen fibers do not fail catastrophically until all collagen fibers are fully recruited and straightened.

## Study Limitations

We reported tension values (force per unit length) in our study as opposed to stress values (force per unit area). This is because thickness varies slightly over the surface of the FM, and thus local areas of stress will likely vary over the surface of the FM as well. Additionally, the cross- sectional area of a ductile material over which the applied force acts changes greatly during loading and thus, the stress is difficult to measure. Due to the difficulty of measuring the change in cross-sectional area of the FM under loading and since performing thickness measurements over the entire surface of the FM is not feasible, tension values were which do not vary over the surface of the membrane were reported. Further,

while stress may vary due to thickness variations within the FM, a state of equi-tension is a reasonable assumption. Due the random distribution of collagen fibers within the FM and thus, the effective isotropic behavior of the FM, tension over the surface of the membrane will be the same in all directions. This feature is essential for the accommodation of fetal movement throughout gestation. If the fibers were strongly aligned in a preferred direction, the collagen fibers would only support the fetal movement in one direction (i.e. the preferred fiber direction). Thus, the FM would likely more often rupture aberrantly with minimal force.

As discussed in the methods section, collagen fiber architecture was quantified at 0mmHg, 5mmHg, 20mmHg, 50mmHg, 80mmHg, 100mmHg, after which it was measured in 10mmHg pressure increments until membrane rupture. The 10mmHg increment was chosen because the rupture pressure in individual specimens was unknown due to specimen variability. If a smaller increment was chosen, total test time would drastically increase the experimental time. Thus, 10mmHg increments of pressure were applied. The fact that no flaws prior to failure were detected with the current 10 mmHg increment should not be construed as an experimental flaw. While finer pressure increments may have shown point defects, it is far more likely that there were none.

Finally, the FM is a delicate tissue and is susceptible to deformation during handling. In order to minimize the impact on measure outcomes, the FM was subjected to minimal handling throughout testing. While performing *in-vitro* surface area measurements, tissue fragments were maintained in a pan of PBS. The fragments were never handled while surface area measurements were being made and were only handled during cutting and transferring tissue to pans of PBS. During mechanical testing, the cylinder of the membrane inflation device is slightly overfilled such that during set-up the membrane is floating on a thin layer of water and not suctioned against the surface of the testing device. While it is inevitable that any handling results in some deformation of the tissue, the reported physiological areal stretch are more than those reported in the literature (3.26 vs. 1.7-2.1). If the reported *in-vivo* areal stretch values in this study were much less than values reported in literature, one could argue that the FM was severely deformed during handling, but that is not the case. Additionally, during mechanical testing, the FM was capable of being stretched more than the estimated *in-vivo* areal stretch 3.26 and up to 4.68. If the FM was severely deformed during test set up, it would likely not stretch up to or more than the estimated *in-vivo* areal stretch and a limited “toe region” would be present on the tension-stretch curve, which did not occur. Thus, deformation associated with handling was minimal.

## Conclusion

In conclusion, the FM is significantly distended *in-vivo*. The derived tension-areal stretch curve and structural measurements show that the FM collagen fibers were rapidly recruited and function near the failure region. Minimal stretch past the physiological stretch results in an acute increase in tension facilitating rapid, catastrophic failure. These architectural and mechanical features underscore how the FM is intrinsically designed to withstand loading yet also undergo catastrophic *programmatic failure*.

## Acknowledgments

We would like to thank the nursing and medical staff of the Labor and Delivery suite and the MRI technical staff of MetroHealth Medical Center. E.M. Joyce was supported in part by a Provost Doctoral Scholarship of the University of Pittsburgh.

Support: NIH HD48467, March of Dimes 21-FY11-9 and Burroughs Wellcome Fund to JJM

## References

1. Blencowe H, Cousens S, Oestergaard MZ, Chou D, Moller A, Narwal R, Adler A, Garcia CV, Rohde S, Say L, Lawn JE. National, regional, and worldwide estimates of preterm birth rates in the year 2010 with time trends since 1990 for selected countries: a systematic analysis and implications. Lancet. 2012; (379):2162–72. [PubMed: 22682464]
2. Liu L, Johnson H, Clousens S. for the Child Health Epidemiology Reference Group of WHO and UNICEF. Global, regional, and national causes of child mortality: an updated systematic analysis for 2010 with time trends since 2000. Lancet. 2012 Published online May 11. 10.1016/S0140-6736(12)60560-1
3. Joyce AM, Hamilton BE, Osterman MJK, Curtin SC, Mathews TJ. Births :Final data for 2013. National Vital Statistics Reports. 2015; 64(1):1–68.
4. Moore RM, Mansour JM, Redline RW, Mercer BM, Moore JJ. The physiology of fetal membrane rupture: insight gained from the determination of physical properties. Placenta. 2006; 27:1037–51. [PubMed: 16516962]
5. Malak TM, Bell SC. Structural characteristics of term human fetal membranes: a novel zone of extreme morphological alteration within the rupture site. Br J Obstet Gynaecol. 1994 May; 101(5): 375–86. [PubMed: 8018607]
6. McLaren J, Taylor DJ, Bell SC. Increased incidence of apoptosis in non-labour – affected cytotrophoblast cells in term fetal membranes overlying the cervix. Human Reprod. 1999; 14(1): 2895–900.
7. McParland PC, Taylor DJ, Bell SC. Mapping of zones of altered morphology and chorionic connective tissue cellular phenotype in human fetal membranes (amniochorion and decidua) overlying the lower uterine pole and cervix before labor at term. Am J Obstet Gynecol. 2003 Nov; 189(5):1481–8. [PubMed: 14634589]
8. McLaren J, Malak TM, Bell SC. Structural characteristics of term human fetal membranes prior to labour: identification of an area of altered morphology overlying the cervix. Hum Reprod. 1999 Jan; 14(1):237–41. [PubMed: 10374127]
9. McLaren J, Taylor DJ, Bell SC. Prostaglandin E(2)-dependent production of latent matrix metalloproteinase-9 in cultures of human fetal membranes. Mol Hum Reprod. 2000 Nov; 6(11): 1033–4. [PubMed: 11044467]
10. McLaren J, Taylor DJ, Bell SC. Increased concentration of pro-matrixmetalloproteinase 9 in term fetal membranes overlying the cervix before labor:implications for membrane remodeling and rupture. Am J Obstet Gynecol. 2000; 182(2):409–16. [PubMed: 10694345]
11. Reti NG, Lappas M, Riley C, Wlodek ME, Permezel M, Walker S, Rice GE. Why domembranes rupture at term? Evidence of increased cellular apoptosis in thesupracervical fetal membranes. Am J Obstet Gynecol. 2007; 196(5):484.e1–10. [PubMed: 17466714]
12. El-Khwad M, Stetzer B, Moore RM, Kumar D, Mercer B, Arikat S, Redline RW, Mansour JM, Moore JJ. Pre-labor fetal membranes have a weak zone overlying the lower uterine pole and cervix. Biol Reprod. 2005; 72:720–726. [PubMed: 15548732]
13. El-Khwad M, Stetzer B, Moore RM, Kumar D, Arikat S, Redline RW, Mansour JM, Moore JJ. A circumscribed area along the tear line in human fetal membranes of vaginal deliveries demonstrates marked physical weakness and coincident evidence of apoptosis and remodeling. JSGI. 2006; 13:191–5.
14. Connon CJ, Nakamura T, Hopkinson A, Quantock A, Yagi N, Doutch J, Meek KM. The biomechanics of amnion rupture: and X-ray diffraction study. PLoS ONE. 2007; 2(11):e1147. [PubMed: 18188405]

15. Lim R, Barker G, Lappas M. SLIT3 is increased in supracervical human foetal membranes and in labouring myometrium and regulates pro-inflammatory mediators. Am J Reprod Immunol. 2014 Apr; 71(4):297–311. [PubMed: 24286238]
16. Chai M, Walker SP, Riley C, Rice GE, Permezel M, Lappas M. Effect of supracervical apposition and spontaneous labour on apoptosis and matrix metalloproteinases in human fetal membranes. Biomed Res Int. 2013; 2013:316146. Epub 2013 Sep 11. 10.1155/2013/316146 [PubMed: 24106700]
17. Lappas M, Odumetse TL, Riley C, Reti NG, Holdsworth-Carson SJ, Rice GE, Permezel M. Pre-labour fetal membranes overlying the cervix display alterations in inflammation and NF-kappaB signalling pathways. Placenta. 2008; 29(12):995–1002. [PubMed: 18952281]
18. Lappas M, Clyde Riley C, Rice GE, Permezel M. Increased Expression of ac-FoxO1 Protein in Prelabor Fetal Membranes Overlying the Cervix: Possible Role in Human Fetal Membrane Rupture. Reprod Sci. 2009; 16(7):635–641. [PubMed: 19293131]
19. Oyen ML, Cook RF, Calvin SE. Mechanical failure of human fetal membrane tissues. J Mater Sci Mater Med. 2004; 15:651–8. [PubMed: 15346731]
20. Oyen ML, Cook RF, Stylianopoulos T, Barocas VH, Calvin SE, Landers DV. Uniaxial and biaxial mechanical behaviour of human amnion. J Mater Res. 2005; 20(11):2902–9.
21. Oyen ML, Calvin SE, Landers DV. Premature rupture of the fetal membranes: is the amnion the major determinant? Am J Obstet Gynecol. 2006 Aug; 195(2):510–5. [PubMed: 16647685]
22. Parry S, Strauss JF 3rd. Premature rupture of the fetal membranes. N Engl J Med. 1998; 338(10): 663–70. [PubMed: 9486996]
23. Mauri A, Ehret AE, Perrini M, Maake C, Ochsenbein-Kölble N, Ehrbar M, Oyen ML, Mazza E. Deformation mechanisms of human amnion: Quantitative studies based on second harmonic generation microscopy. J Biomech. 2015 Feb 7. Epub ahead of print. 10.1016/j.jbiomech. 2015.01.045
24. Strauss JF 3rd. Extracellular matrix dynamics and fetal membrane rupture. Reprod Sci. 2013 Feb; 20(2):140–53. Epub 2012. 10.1177/1933719111424454 [PubMed: 22267536]
25. Alger LS, Pupkin MJ. Etiology of preterm premature rupture of the membranes. Clin Obstet Gynecol. 1986 Dec; 29(4):758–70. [PubMed: 3545583]
26. Millar LK, Stollberg J, DeBuque L, Bryant-Greenwood G. Fetal membrane distention: determination of the intrauterine surface area and distention of the fetal membranes preterm and at term. Am J Obstet Gynecol. 2000 Jan; 182(1 Pt 1):128–34. [PubMed: 10649167]
27. Kumar D, Fung W, Moore RM, et al. Proinflammatory cytokines found in amniotic fluid induce collagen remodeling, apoptosis, and biophysical weakening of cultured human fetal membranes. BiolReprod. 2006; 74:29–34.
28. Moore RM, Novak JB, Kumar D, Mansour JM, Mercer BM, Moore JJ. Alpha-lipoic acid inhibits Tumor Necrosis Factor-induced remodeling and weakening of human fetal membranes. Biol Reprod. 2009; 80:781–7. [PubMed: 19109223]
29. Moore RM, Schatz F, Kumar D, et al. Alpha-Lipoic Acid Inhibits Thrombin-Induced Fetal Membrane Weakening In Vitro. Placenta. 2010; 31:886–892. [PubMed: 20709392]
30. Kumar D, Schatz F, Moore RM, et al. The effects of thrombin and cytokines upon the biomechanics and remodeling of isolated amnion membrane, in vitro. Placenta. 2011; 32:206–213. [PubMed: 21300402]
31. Puthiyachirakkal M, Lemerand K, Kumar D, et al. Thrombin weakens the amnion extracellular matrix (ECM) directly rather than through protease activated receptors. Placenta. 2013; 34:924–31. [PubMed: 23953865]
32. Kumar D, Moore RM, Nash A, Springel E, et al. Decidual GM-CSF is a critical common intermediate necessary for thrombin and TNF induced *in-vitro* fetal membrane weakening. Placenta. 2014; 35:1049–1056. [PubMed: 25454284]
33. Kumar D, Springel E, Moore RM, Mercer BM, Philipson E, Mansour JM, Mesiano S, Schatz F, Lockwood CJ, Moore JJ. Progesterone inhibits in-vitro fetal membrane weakening. Am Journal Obstet and Gynecol. AJOG. 201510.1016/j.ajog.2015.06.014
34. Ellsmere JC, Khanna RA, Lee JM. Mechanical loading of bovine pericardium accelerates enzymatic degradation. Biomaterials. 1999; 20:1143–50. [PubMed: 10382830]

35. Coulson WF. The effect of proteolytic enzymes on the tensile strength of whole aorta and isolated aortic elastin. Biochim Biophys Acta. 1971; 237:378–86. [PubMed: 4105895]
36. Huang C, Yannas IV. Mechanochemical studies of enzymatic degradation of insoluble collagen fibers. J Biomed Mater Res Symp. 1977; 8:137–54.
37. Adhikari AS, Chai J, Dunn AR. Mechanical load induces a 100-fold increase in the rate of collagen proteolysis by MMP-1. J Am Chem Soc. 2011; 133(6):1686–1689. [PubMed: 21247159]
38. Sacks MS, Smith DB, Hiester ED. A small angle light scattering device for planar connective tissue microstructural analysis. Ann Biomed Eng. 1997; 25(4):678–89. [PubMed: 9236980]
39. Sacks MS. Small-angle light scattering methods for soft connective tissue structural analysis. Encyclopedia of biomaterials and biomedical engineering. 2004
40. Derganc J, Bozic B, Svetina S, Zeks B. Stability analysis of micropipette aspiration of neutrophils. Biophys J. 2000; 79(1):153–62. [PubMed: 10866944]
41. Joyce EM 1, Moore JJ, Sacks MS. Biomechanics of the fetal membrane prior to mechanical failure: review and implications. Eur J Obstet Gynecol Reprod Biol. 2009; 144(Suppl 1):S121–7. Epub 2009 Mar 19. 10.1016/j.ejogrb.2009.02.014 [PubMed: 19303191]
42. Parry-Jones E, Priya S. A study of the elasticity and tension of fetal membranes and of the relation of the area of the gestational sac to the area of the uterine cavity. Br J Obstet Gynaecol. 1976 Mar; 83(3):205–12. [PubMed: 1252386]
43. Reece IJ, van Noort R, Martin TR, Black MM. The physical properties of bovine pericardium: a study of the effects of stretching during chemical treatment in glutaraldehyde. Ann Thorac Surg. 1982; 33(5):480–5. [PubMed: 6805445]
44. Crofts CE, Trowbridge EA. The tensile strength of natural and chemically modified bovine pericardium. J Biomed Mater Res. 1988; 22:89–98. [PubMed: 3128550]
45. Zioupos P, Barbenel JC, Fisher J. Mechanical and optical anisotropy of bovine pericardium. Med Biol Eng Comput. 1992; 30:76–82. [PubMed: 1640759]
46. Sacks MS, Mirnajafi A, Sun W, Schmidt P. Bioprosthetic heart valve heterograftbiomaterials: structure, mechanical behavior and computational simulation. Expert Rev Med Devices. 2006; 3(6):817–34. [PubMed: 17280546]
47. Thorton GM, Schwab TD, Oxlan TR. Cyclic loading causes faster rupture andstrain rate than static loading in medial collateral ligament at high stress. Clin Biomech. 2007; 22:932–40.
48. Bartel, DL.; Davy, DT.; Keaveny, TM. Orthopaedic biomechanics mechanics and design in musculoskeletal systems. Upper Saddle River: Pearson Education; 2006. p. 371
49. Ota A, Yonemoto H, Someya A, Itoh S, Kinoshita K, Nagaoka I. Changes in matrix metalloproteinase 2 activities in amniochorions during premature rupture of membranes. J Soc Gynecol Investig. 2006; 13(8):592–7.
50. Yonemoto H, Young CB, Ross JT, Guilbert LL, Fairclough RJ, Olson DM. Changes in matrix metalloproteinase (MMP)-2 and MMP-9 in the fetal amnion and chorion during gestation and at term and preterm labor. Placenta. 2006; 27(6-7):669–77. Epub 2005 Aug 2. [PubMed: 16061282]
51. Goldman S, Weiss A, Eyali V, Shalev E. Differential activity of the gelatinases (matrix metalloproteinases 2 and 9) in the fetal membranes and decidua, associated with labour. Mol Hum Reprod. 2003; 9(6):367–73. [PubMed: 12771238]

## Highlights

- *In-vivo* fetal membrane stretch was determined utilizing MRI imaging.
- Fetal membrane collagen fibers function near their failure state at term.
- The physiological surface area at term is approximately 70% of that at rupture.

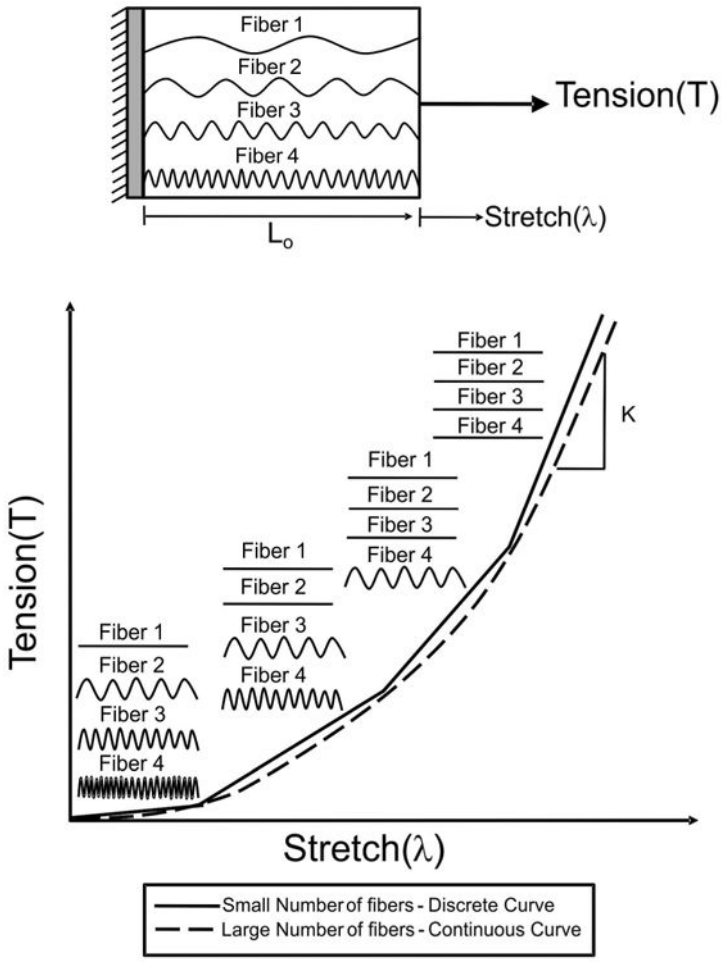


**Figure 1.**

FM collagen fiber recruitment: Traditional recruitment modeling assumes that a collagen fiber does not bear load until the collagen fiber is straightened, where K is the elastic constant. Gradual recruitment of collagen fibers results in a non-linear tension-stretch relationship. Initially all collagen fibers are crimped and do not bear load, which results in the toe region. With increased stretch, the fiber with the least amount of crimp, fiber 1 in this schematic, will bear load and become straightened. With increased stretch, fibers 2 and 3 will become straightened, causing the tension-stretch curve to increase in a non-linear manner. As stretch continues to increase, all collagen fibers (1, 2, 3, and 4) will bear load and become straightened resulting in a highly linear region on the tension-stretch curve. When a small population of fibers is present, the tension-stretch curve is discrete (indicated by the solid line), but when a large population of fibers exists, the tension-stretch curve is continuous (dashed line).

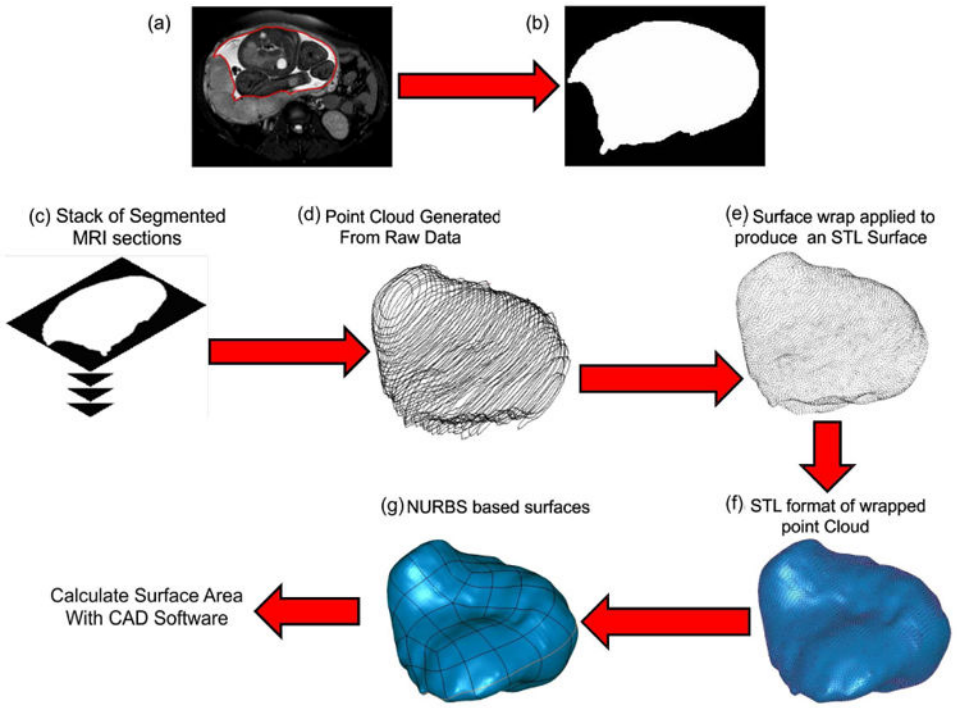


**Figure 2.**

Key steps in the three dimensional reconstruction process: The FM (not including the placenta) in (a) each MRI section is (b) outlined and converted to a black and white image, referred to as segmentation. (c) After each MRI section of the entire FM is segmented, the segments are then (d) imported into Geomagic/Studio in order to generate a point cloud. (e) Next, a surface wrap is mathematically applied in order to generate a stereolithography (STL) surface. (f) The STL surface is a simple surface definition made by triangulating the point cloud from data, which produces a set of triangular elements that only contains information of connectivity and surface normals. (g) Finally, a Non Uniform Rational B-spline (NURBs) based surface is constructed, which is compatible with commercial CAD modeling tools, such as SolidWorks which can calculate the desired surface area.

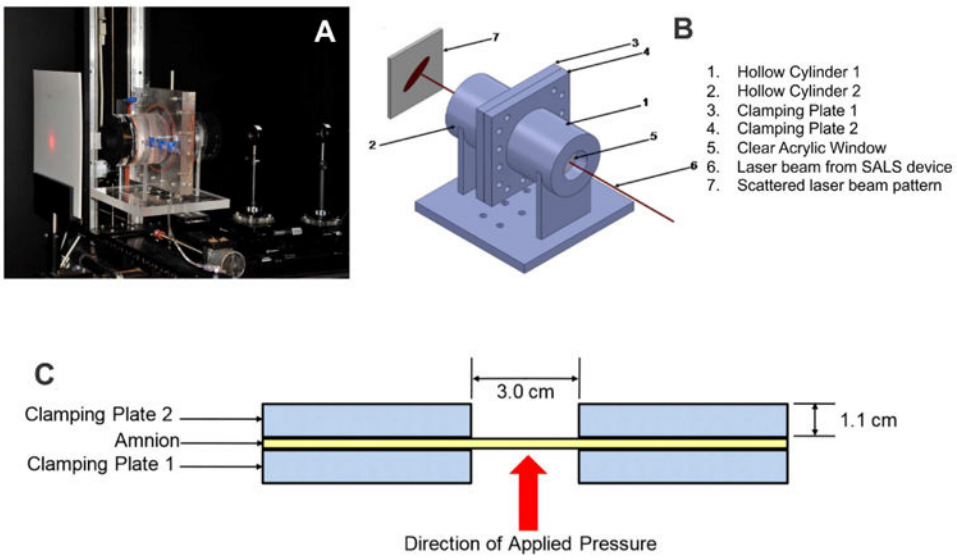


**Figure 3.**

Membrane inflation device: (A) Image of the membrane inflation device. (B) Schematic of the membrane inflation device. The device consisted of hollow cylinders (1 and 2) attached to clamping plates (3 and 4), which hold the FM fragment between them during inflation. Each cylinder (1 and 2) contains a clear acrylic window (5). (C) The diameter of the membrane inflation device is 3.0 cm.

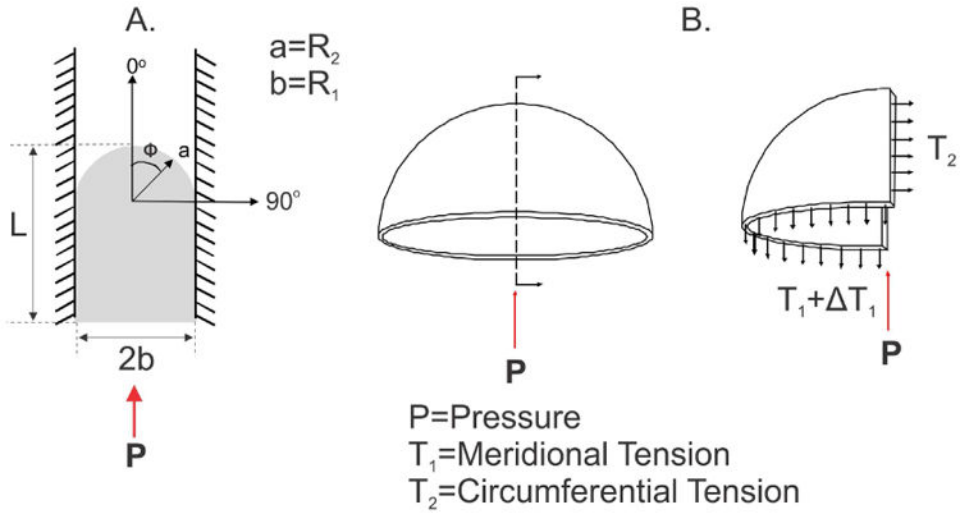


**Figure 4.**

Determination of membrane tension: (A) An inflated membrane, confined by the walls of the membrane inflation device with the coordinate system used to determine membrane tension, where φ is between 0° and 90°, L is the measured displacement of the center of the inflated FM; a ($R_2$) is the radius of the deformed membrane; b ($R_1$) is the radius of the membrane inflation device; and P is the applied pressure. (B) A free body diagram of the meridional stress resultant ($T_1$) and the circumferential stress resultant ($T_2$).

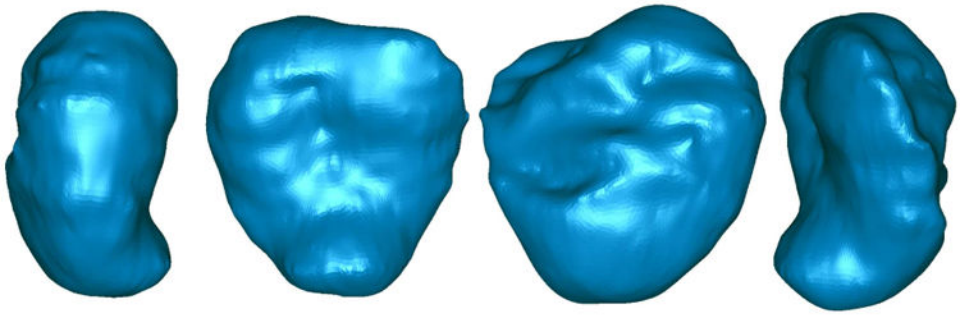

**Figure 5.**

Three dimensional reconstruction from MRI: A representative image of three dimensional reconstruction of one FM from MRI using the process diagramed in Figure 2. This is a 360° view of a single membrane.

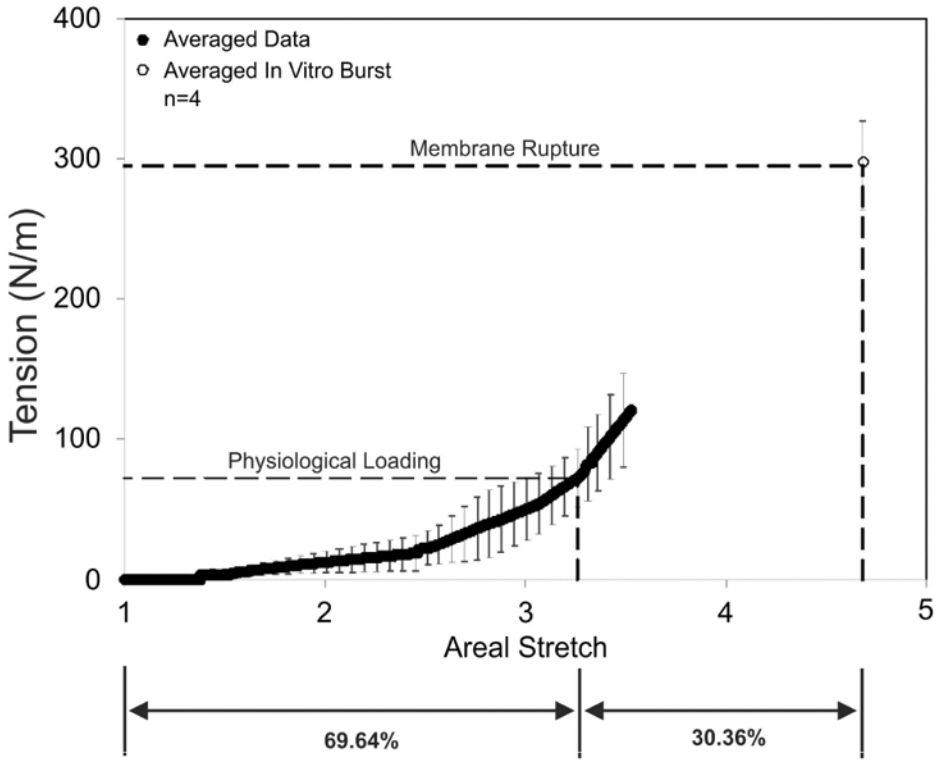


**Figure 6.**

The FM tension-areal stretch curve: The *in-vivo* deformation determined was 3.26±0.11, which corresponds to a tension value of 76.26 N/m. The average rupture tension was 295.08 ± 31.73 N/m, which is represented by the open circle. The solid black circles represent the averaged data. The dashed lines designate the physiological loading (*in-vivo* deformation) as well as membrane rupture.

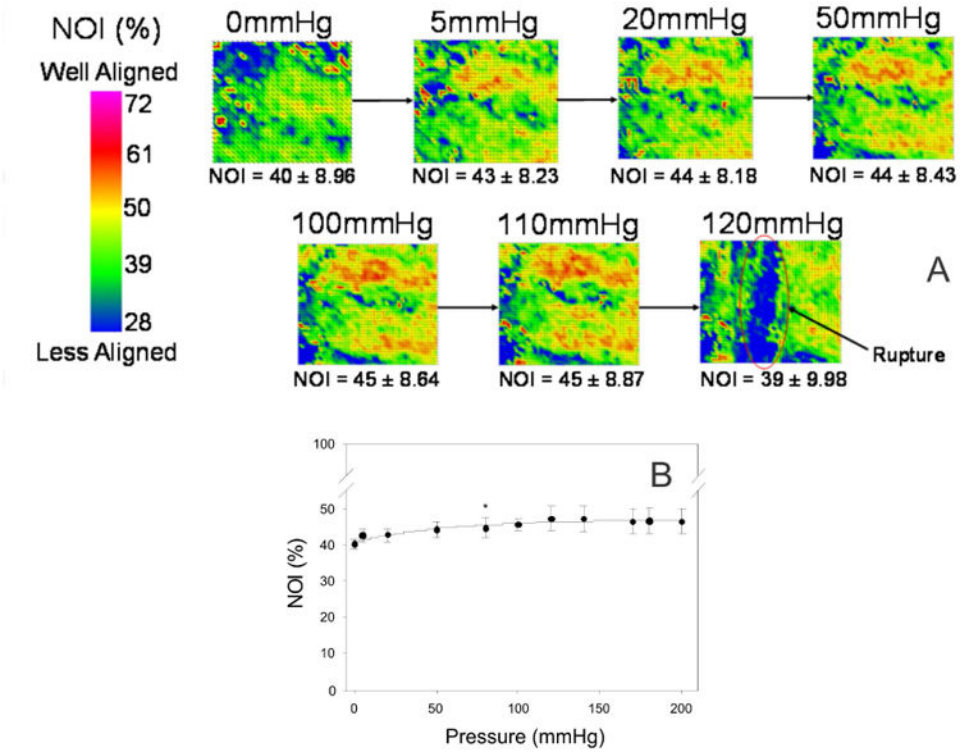


**Figure 7.**

Quantitative fiber architectural measurements: (A) Representative image of the microstructural changes that occur in the amnion layer of the FM under isotropic loading. NOI values increased with increased pressure. However these changes were not found to be statistically significant. Since the change in preferred direction was not significant, the increase in fiber alignment was likely due to the uncrimping of the collagen fibers. Most importantly, failure of the amnion layer was found to be catastrophic. Point defects did not appear in the tissue leading up to failure. (B) These results can also be graphically presented. The NOI increase with increased pressure, with the greatest change in NOI occurs under the first 5 mmHg. NOI continually increases with pressure up to 100 mmHg, with minimal change thereafter.

**Table 1**

**Summary of measurements in 8 patients**

| | FM surface area ($cm^2$) | | | | | | FM stretch and rupture | | |
|---|---|---|---|---|---|---|---|---|---|
| **(n=8)** | ***In-vitro* disc** | ***In-vitro* Reflected FM** | ***In-vitro* Total** | ***In-vivo* disc** | ***In-vivo* Reflected FM** | ***In-vivo* Total** | **FM stretch** | **Disc Stretch** | **Rupture pressure (mmHg)** |
| 1 | 265 | 505 | 771 | 254.23 | 1663.07 | 1917 | 3.29 | 0.96 | 242 |
| 2 | 252 | 565 | 817 | 309.20 | 1582.50 | 1892 | 2.80 | 1.23 | 210 |
| 3 | 300 | 578 | 878 | 372.27 | 1904.73 | 2277 | 3.30 | 1.24 | 240 |
| 4 | 432 | 616 | 1048 | 416.33 | 2311.67 | 2728 | 3.75 | 0.96 | 257 |
| 5 | 267 | 430 | 697 | 504.66 | 1438.34 | 1943 | 3.34 | 1.89 | 428 |
| 6 | 278 | 597 | 875 | 304.20 | 2108.50 | 2413 | 3.53 | 1.09 | 280 |
| 7 | 243 | 587 | 829 | 310.46 | 1686.84 | 1997 | 2.88 | 1.28 | 400 |
| 8 | 341 | 485 | 826 | 385.42 | 1531.68 | 1917 | 3.16 | 1.13 | 364 |
| Mean ± SEM | 297.18 ± 22.14 | 545.41 ± 22.09 | 842.59 ± 35.86 | 357.09 ± 28.08 | 1778.42 ± 107.39 | 2135.51 ± 108.47 | 3.26 ± 0.11 | 1.22 ± 0.10 | 302.63 ± 29.19 |